JOURNAL OF
ENVIRONMENTAL HYDROLOGY
The Electronic Journal of the International Association for Environmental Hydrology
On the World Wide Web at http://www.hydroweb.com
VOLUME 12 2004

DEM-RS-GIS BASED STORM RUNOFF HYDROGRAPH ESTIMATION FOR THE HEART RIVER SUB-BASIN, MISSOURI RIVER BASIN

Assefa M. Melesse | Earth Systems Science Institute, University of North Dakota
Grand Forks, North Dakota, USA

Accurate representation of the physical and biological features of the landscape within the watershed is required as the extent and type of watershed cover affects the movement of water in the hydrologic cycle. Remote sensing (RS), such as satellite imagery from Landsat and other satellites, provides land-cover and surface microclimate information with high temporal and spatial accuracy. The use of these data to understand hydrologic processes depends on how accurately they are interpreted and mapped. A study conducted at the Heart River sub-basin in the Missouri River basin, located on southwestern North Dakota, utilizes Landsat Enhanced Thematic Mapper Plus imagery and geographic information system (GIS) tools to derive land-cover for the summer of 2002. Land surface temperature and Normalized Difference Vegetation Index (NDVI) from the Landsat image was used to better map the land-cover and estimate runoff response. The corresponding infiltration excess runoff response of the study area was estimated using the United States Department of Agriculture, Natural Resources Conservation Service Curve Number (USDA-NRCS-CN) method. A Digital Elevation Model (DEM)-RS-GIS routing technique based on a 1-D kinematic wave approximation was developed to predict stream response to runoff events based on the travel time from each grid cell to the watershed outlet. Simulated and observed runoff volume and hydrographs were compared for three storm events. The NRCS-CN method with the DEM-RS-GIS routing technique predicts the observed runoff volume with mean error and residual standard deviation of (–38% and 5 mm), peak flow (-15% and 2.38 m^3/sec), and time to peak flow (17% and, 1.26 day), respectively.

INTRODUCTION

Watershed models are tools that integrate our knowledge of hydrologic systems to simulate real world hydrologic processes. The primary objective of these models is to ascertain the impact of changes in land-use and management practices on water quality and quantity. Lumped watershed models have been used traditionally to analyze the conversion of excess rainfall into surface runoff. These models assumed that excess rainfall and hydrologic parameters are uniform over the watershed, and that the rainfall-runoff process is linear, and can be predicted using unit hydrograph theory. The unit hydrograph theory treats the watershed as a lumped linear system in which an input function (excess rainfall hyetograph) is acted on by a transfer function (the unit hydrograph) to produce an output response (stream flow hydrograph). The unit hydrograph is estimated using observed empirical data and requires the estimation of specific watershed. In practice, the excess rainfall and hydrologic parameters over a large watershed are nonuniform. To overcome this deficiency, spatially distributed models have been developed (Ott, et al., 1991; Ogden, 1997; Olivera and Maidment, 1999) in which the watershed is divided into a number of sub-watersheds or cells with spatially variable excess rainfall and hydrologic parameters.

Distributed-parameter models divide the entire watershed into smaller sub-basins or grids which are assumed to have uniform hydrologic characteristics. Water and pollutants are routed through each of the cells and through the outlet. Distributed-parameter models may be accurate and also offer the possibility of a significant improvement over lumped models because they can model the spatial variability of hydrologic parameters. These parameters can be derived from remote sensing of various platforms (ground-based, airborne or space borne) and sensors (Landsat Thematic Mapper, TM), and Enhanced Thematic Mapper Plus, ETM+).

Remote Sensing Application

Remote Sensing (RS) plays an increasing role in runoff modeling because of the potential to observe the entire watershed rather than merely points, and also because of the potential to make entirely new measurements of hydrologic variables not generally possible with traditional techniques. Although RS cannot be used directly to quantify runoff, it can be used to determine watershed geometry, drainage network, and also hydrologic input parameters such as soil moisture or delineated land-use classes that are used to define runoff coefficients. The most promising applications of RS data in hydrologic modeling are providing areal information on hydrometereological variables such as precipitation and land surface temperature, land-cover classes, and vegetation and basin characteristics. Land-cover determination using RS is widely used for large watersheds and when land-cover (actual distribution of physical features of land) information is required at times of the year when such data is critical.

Accurate and up-to-date information on land-cover and the state of the environment are critical components of flood management, environmental planning, and management. Land-cover information is used in watershed modeling to estimate the value of surface roughness or friction as it affects the velocity of the overland flow of water. It may also be used to determine the amount of rainfall infiltration on a surface. RS-based surface climate parameters computed from radiance data provide distribution of vegetation or surface imperviousness at micro or pixel level. The pixel format of digital RS data makes it suitable to merge with a geographic Information System (GIS). GIS allows for the combination of remotely-sensed data with other spatial data forms such as topography, soils maps and hydrologic variables such as rainfall distribution and soil moisture.

Geographic Information System Application

GIS is a computer-based tool that displays, stores, analyzes, retrieves and generates spatial and nonspatial (attribute) data. GIS technology is a well-established tool used in hydrologic modeling, which facilitates processing, management, and interpretation of all available data. It also provides a practical means for modeling and analyzing the spatial characteristics of the hydrologic cycle.

Several studies have been done to incorporate GIS in hydrologic modeling of watersheds. These studies have different scopes and can be generally grouped into four categories:

- Computation of input parameters for existing hydrologic models (Muzik and Pomeroy, 1990; Stube and Johnson, 1990; Djokic and Maidment, 1991; Olivera and Maidment, 1999; Vieux, 2001).
- Mapping and display of hydrologic variables (Moeller, 1991; Ragan and Kosicki, 1991; Mueschen and Steinnocher, 2000).
- Watershed surface representation (Sasowsky and Gardner, 1991; Moore and Grayson, 1991; Smith and Brilly, 1992).
- Identification of hydrologic response units (See et al, 1992; Flugel, 1995; Mueschen and Steinnocker, 2000; Vieux, 2001).

Maidment (1993b) pointed out an alternative scheme to classify the different contributions of GIS in hydrology: hydrologic assessment, hydrological parameter estimation, loosely-coupled GIS and hydrological models, and integrated GIS and hydrological models.

Maidment (1992a, 1992b, and 1993a) introduced a procedure using raster GIS and a time-area method to derive a spatially distributed unit hydrograph. Maidment used the Digital Elevation Model (DEM) of the watershed to determine the flow direction from each cell based on the maximum downhill slope. Flow velocity through each cell was estimated based on the kinematic wave assumption, then the flow time through each cell was obtained by dividing the flow distance by the flow velocity. Maidment's procedure was applied to watersheds in the Canadian Rockies using GRASS GIS (Muzik, 1995 and Ajward, 1996).

In this study, an integrated technique employing RS (satellite imagery) to derive level 1 (Anderson et al., 1976) land-cover classes computed from Landsat ETM+ image, the USDA, Natural Resources Conservation Services-Curve Number (NRCS-CN) technique to compute excess rainfall, and grid GIS to compute hydrologic parameters from DEM, is presented which predicts spatially distributed excess rainfall volume and routes the water to the watershed outlet. A grid GIS-based routing technique based on travel time is developed to generate the direct runoff hydrograph without relying on unit hydrograph theory. The methodology is demonstrated and validated using data measured in the Heart River sub-basin located in the Missouri River basin, southwestern North Dakota.

The overall objective of the study is to develop a DEM-RS-GIS runoff hydrograph prediction technique applied to the Heart River sub-basin in the Missouri River basin in southwestern North Dakota.

The specific objectives are to (1) develop Landsat-based land-cover, (2) develop the storm runoff hydrograph using a spatially distributed travel time technique, and (3) verify the predicted runoff (volume and hydrograph) with observed values.

STUDY AREA AND DATA SETS

Study Area

The area considered in this study is located in the upper Heart River sub-basin of the Missouri River basin in Stark County with a smaller western portion in Dunn County, upstream of Lake Tschida in southwestern North Dakota (Figure 1). The Heart River flows east and contributes to the Missouri River with a drainage area of 807 km^2.

The soil type is a Parshall fine sandy loam which are deep, well-drained soils formed in fine sandy loam alluvium on terraces and outwash plains and in upland swales. The surface layer and subsoil is dark grayish-brown fine sandy loam. The underlying material is dark grayish-brown fine sandy loam and loamy fine sand. Permeability is moderately rapid. The average annual precipitation is 406 mm; increasing from west to east for this semiarid area. Rainfall is highest from late spring to

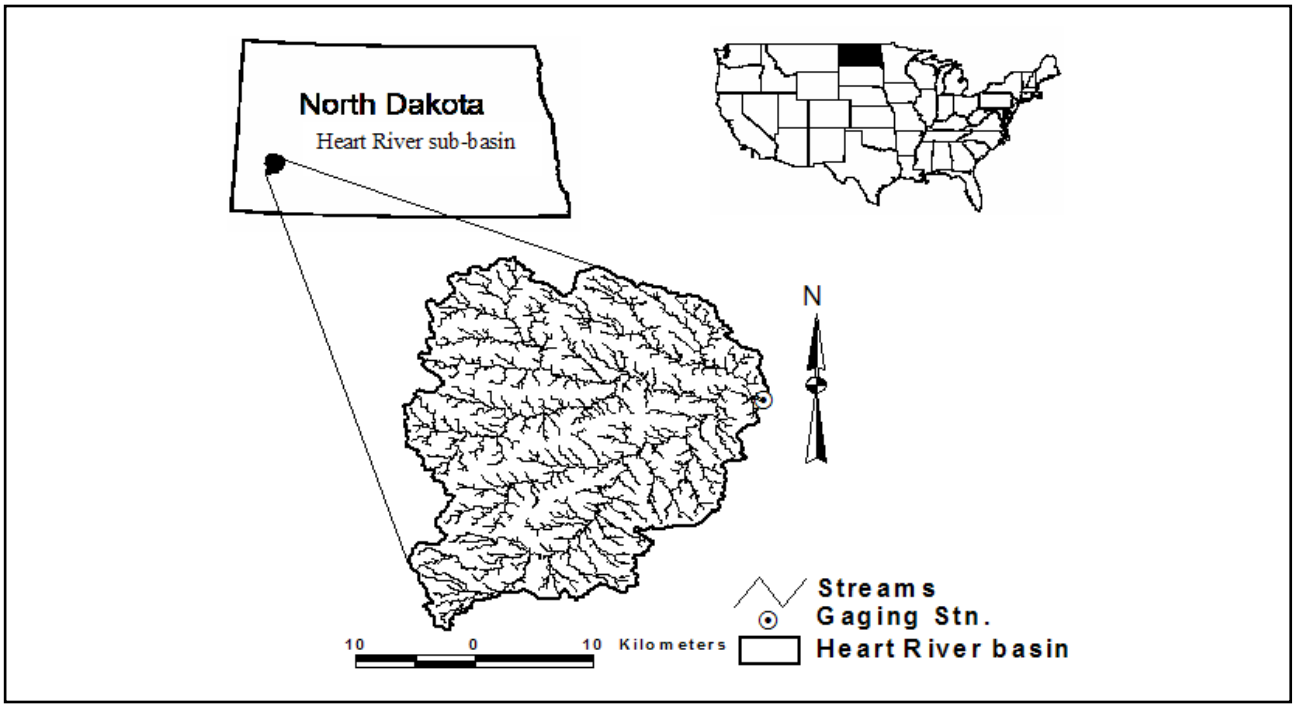

Figure 1. Location of the Heart River sub-basin.

midsummer and very low during the rest of the year. Winter precipitation is snow. Average annual temperature is 4.4-7.2 ^oC. Average freeze-free period is 110 to 135 days.

Data Sets

Land-cover classes were derived from a September 11, 2002 Landsat ETM+ image of the Heart River. Because Landsat satellites have sun-synchronous orbit and nadir-pointed instrument, the Landsat image was acquired at approximately midmorning local time. The Level-1G/systematic corrected scene product image was subsequently geocorrected (affine method) to base map (1:24,000 scale vector roads), and unsupervised classification of the image was accomplished using the Iterative Self-Organizing Data Analysis Technique (ISODATA) (Tou and Gonzales, 1974) algorithm from ERDAS IMAGINE (ERDAS, 1999) after radiometric correction was made and converted to reflectance.

A resampled 100-m resolution DEM was obtained from the United States Geological Survey (USGS) (USGS, 2003) for the Heart River sub-basin (Figure 2). An ArcView Avenue script was

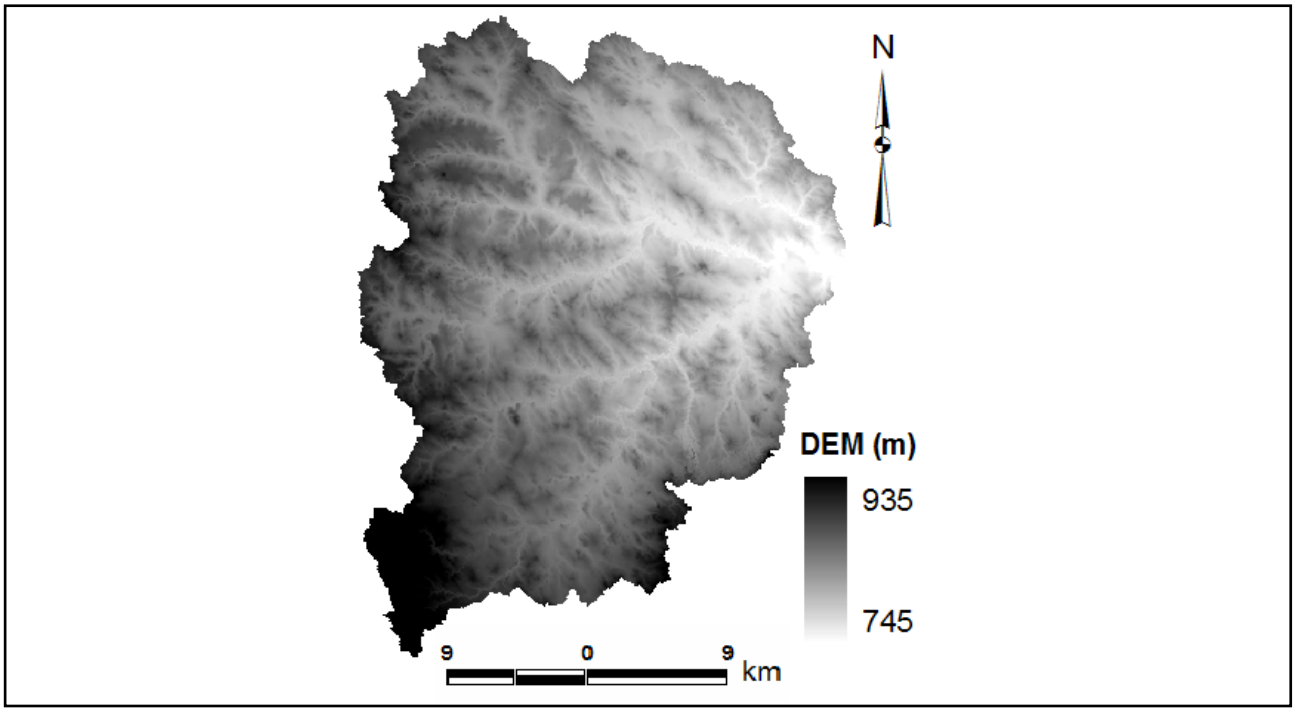

Figure 2. Digital Elevation Model (100-m) of the Heart River sub-basin.

written to process the DEM and generate the hydrologic parameters required to develop the spatially distributed travel time distribution and direct runoff hydrographs by routing the runoff down to the outlet.

The soils GIS layer showing Hydrologic Soils Group (HSG) was obtained from USDA - States Soils Geographic (STATSGO) database (Figure 3). Since the STATSGO database has a scale of 1:250,000 and the soil map unit identification in the database can have more than one HSG, hard copy county level soil survey maps were consulted to improve the accuracy of assigning HSG. Soils are classified into four HSGs (A, B, C, and D) according to their minimum infiltration rate, which is

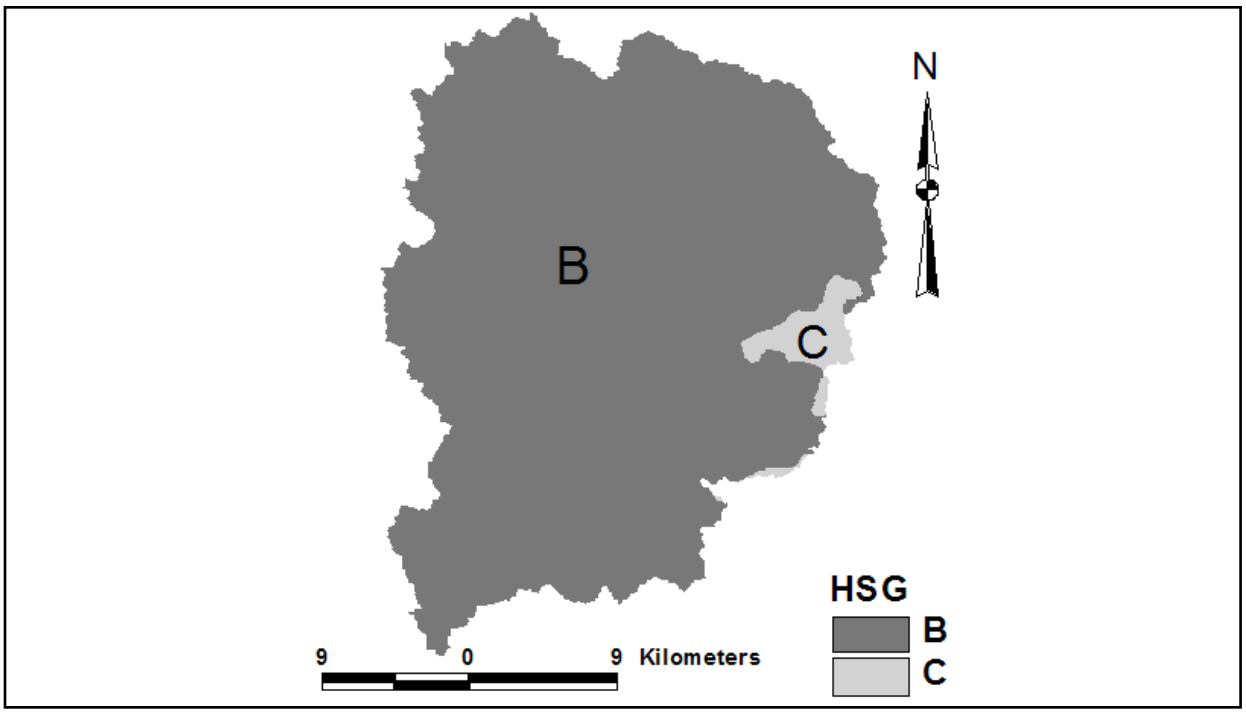

Figure 3. Hydrologic Soils Group (HSG).

obtained for a bare soil after prolonged wetting. Soils in group A have lowest runoff potential, soils in group B have moderately low runoff potential, soils in group C have moderately high runoff potential, and group D soils have the highest runoff potential.

Daily rainfall data were obtained from the Dickinson station of the North Dakota Agricultural Weather Network. Three storms with total volumes of not less than 12.75 mm (0.5 inch) (USDA, 1986) were selected for the study (Table 1). The minimum rainfall volume was selected to be consistent with minimum storm size recommended for use with the NRCS-CN method. The corresponding discharge for each storm was acquired from the USGS (USGS, 2003).

Table 1. Observed Storm and Discharge Events Used in the Study

		Rainfall			**Runoff**			
Storm number	Date	Volume (mm)	Duration (day)	Average Intensity (mm/day)	Volume (mm)	Volume (%)	Peak (m^3/s)	Time to peak (day)
1	01-Jun-02	122.68	11	11.15	21.38	17.4	49.13	13
2	19-Jul-02	48.78	7	6.97	0.92	1.9	1.22	10
3	18-Aug-02	44.70	8	5.59	1.79	4	2.72	9

METHODOLOGY

Land-cover Mapping

The unsupervised ISODATA classifier yielded 30 spectral classes. Figure 4 shows the flow chart for land-cover mapping. Scattergrams of the scaled Normalized Difference Vegetation Index ($NDVI_s$) versus scaled land surface temperature (T_s) were used to find instances of strong correlation with the land-cover data of the sub-basin. The spectral signatures of all these classes were used to determine the mean radiance for each band. From the scattergram, five USGS-Land Use and Land Cover (LULC) system level 1 land-cover classes (Anderson et al., 1976) were identified. Melesse (2002) has demonstrated this technique for three watersheds in Florida of different cover and location. The approach was useful in the absence of ground truth data and the classification technique resulted an overall accuracy of over 80%.

Normalized Difference Vegetation Index

The NDVI (Rouse et al., 1974) is a measure of the amount of greenness in the vegetation cover of a watershed. It is the ratio of the difference to the sum of the reflectance values of near infrared (NIR) (0.76 – 0.91mm) and red (0.62 – 0.7mm) bands (Equation 1).

$$NDVI = \frac{NIR - RED}{NIR + RED} \tag{1}$$

In highly vegetated areas, the NDVI typically ranges from 0.1 to 0.6, in proportion to the density and greenness of the plant canopy. Clouds, water, and snow, which have larger visible reflectance than NIR reflectance, will yield negative NDVI values. Rock and bare soil areas have similar reflectances in the two bands and result in NDVI near zero.

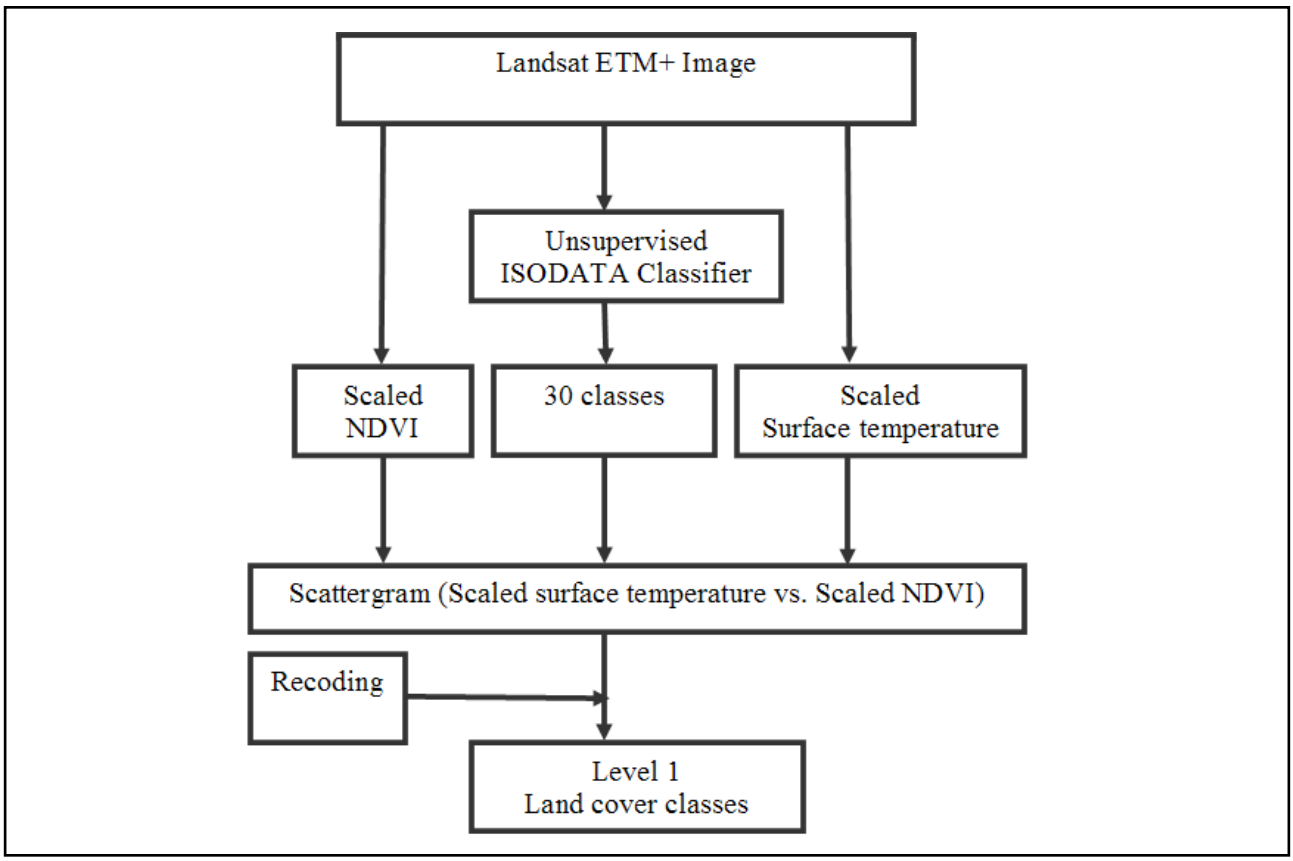

Figure 4. Land-cover classification flow chart.

Studies have shown strong relationships between the biophysical properties (such as leaf biomass) of forests and red and NIR radiance from Landsat TM sensor (Gillies et al., 1997; Melesse et al., 2001).

Scaling NDVI between the low and high values is indicated as,

$$NDVI_S = \frac{NDVI - NDVI_{low}}{NDVI_{high} - NDVI_{low}} \tag{2}$$

$NDVI_s$ ranges between 0 and 1. $NDVI_{low}$ and $NDVI_{high}$ are values for bare soil and dense vegetation respectively.

Surface radiant temperature

Surface temperature is an important parameter in understanding the exchange of energy between the earth surface and the environment. Surface radiant temperatures were calculated from the thermal band radiance values of ETM+ sensor. The surface temperature was obtained from Landsat thermal infrared band using the simplified Planck function (Markham and Barker, 1986),

$$T = \frac{K_2}{\ln\left(\frac{K_1}{R} + 1\right)} \tag{3}$$

where T is surface radiant (at-sensor) temperature (K), R is spectral radiance, K_1 is calibration constant 1; K_2 is calibration constant 2. For Landsat-7 ETM+, K_1 and K_2 are 666.09 $Wm^{-2}sr^{-1}mm^{-1}$ and 1282.71K, respectively.

For Landsat 7 ETM+ sensor R is given as,

$$R = \frac{(L_{\max} - L_{\min})}{254} * (DN - 1) + L_{\min} \quad (4)$$

where, L_{max} and L_{min} are maximum and minimum spectral radiance, ($Wm^{-2}ster^{-1}\mu m^{-1}$) at $DN = 255$ and $DN = 0$, respectively. DN is digital number; L_{max} and L_{min} are non-real time post-launch values, different for the low (6L) and high (6H) gain versions of the thermal band on ETM+.

The scaled surface radiant temperature, T_S, is given by,

$$T_S = \frac{T_i - T_{low}}{T_{high} - T_{low}} \quad (5)$$

where T_i is the surface radiant temperature for pixel i, T_{low} is the lowest surface radiant temperature of the area of analysis and T_{high} is the highest surface radiant temperature.

The NRCS-CN Technique

The infiltration-excess runoff has been studied using the curve number technique. The NRCS-CN approach was developed by USDA-NRCS to predict peak storm runoff on ungaged watersheds. This method is simple and has been used as a method of determining excess rainfall in hydrologic models such as Agricultural Non-Point Source Pollution Model (AGNPS) (Young et al., 1985); Chemical, Runoff, and Erosion from Agricultural Management Systems (CREAMS) (USDA, 1980); Groundwater Loading Effects of Agricultural Management Systems (GLEAMS) (Leonard et al., 1986); and Hydrologic Engineering Center (HEC-1) (U.S. Army Corps of Engineers, 1985). It has also provided a runoff component for a succession of water quality and erosion models including Areal Nonpoint Source Watershed Environment Response System (ANSWERS) (Beasley and Huggins, 1981); the Simulator for Water Resources in Rural Basins (WRRB) (Arnold and Williams, 1995); the Water Erosion Prediction Project (WEPP) (Laflen et al., 1991); and most recently the distributed Soil Water Assessment Tool (SWAT) (Arnold et al., 1998).

In the NRCS runoff equation, the ratio of actual retention to maximum retention is assumed to be equal to the ratio of direct runoff to rainfall minus initial abstraction. This can be expressed mathematically as (USDA, 1985)

$$\frac{F}{S} = \frac{Q}{P - I} \quad (6)$$

where F is actual retention after runoff begins (mm); S is watershed storage (mm) ($S \geq F$); Q is actual direct runoff (mm); P is total rainfall (mm) ($P \geq Q$); I is initial abstraction (mm). The amount of actual retention can be expressed as

$$F = (P - I) - Q \quad (7)$$

The initial abstraction defined by the NRCS mainly consists of interception, depression storage, and infiltration occurring prior to runoff. To eliminate the necessity of estimating both parameters I and S in the above equation, the relation between I and S was estimated by analyzing rainfall-runoff data for many small watersheds. The empirical relationship is

$$I = 0.2S \quad (8)$$

Substituting Equation 8 into Equation 6 and 7 yields

$$Q = \frac{(P - 0.2S)^2}{P + 0.8S} \qquad (P > 0.2S) \tag{9}$$

Which is the rainfall-runoff equation used by the NRCS for estimating depth of direct runoff from storm rainfall. The equation has one variable, P, and one parameter, S. S is related to curve number (CN) by

$$S = \frac{25400}{CN} - 254 \tag{10}$$

The CN is a runoff index based on physical parameters of the watershed. Its value ranges from 1 (minimum runoff) to 100 (maximum runoff). It is determined based on hydrologic soil group, land-use, land treatment, and hydrologic conditions. The antecedent moisture condition (AMC) of the soil is also used to determine CN. Based on antecedent rainfall volumes, three AMC classes AMC I (dry soil), AMC II (normal condition), and AMC III (wet soil) are identified (USDA, 1985). For the three storms used in this study, AMC II was assumed based on 5-days antecedent rainfall volume.

DEM-RS-GIS based Runoff Routing Technique

Topography plays an important role in the distribution and flux of water and energy within the natural landscape. Surface runoff, evaporation, and infiltration are hydrologic processes that take place at the ground-atmosphere interface. The quantitative assessment of these processes depends on topographic configuration of the landscape, which is one of several controlling boundary conditions.

The runoff hydrograph at the outlet of the watershed was predicted by determining abstractions from land-cover, soils, and rainfall information, followed by routing the spatially distributed runoff using topographic data. Spatially distributed direct hydrographs were generated using the concept of travel time distribution. The flow chart summarizing this procedure is shown in Figure 5.

Grid cells are classified into overland and channel cells depending on flow accumulations. If cells are receiving an upstream inflow, they are channel cells, otherwise they are classified as overland cells. Cells on the ridge and outer boundary of the watershed are overland cells. Overland flow does not exist over a flow length of 100 m (Bedient and Huber, 1992) after which flow is concentrated into smaller channels. Flow accumulation of 1 grid cell represents an overland flow length of 100 m or 141 m depending on flow direction.

Overland flow

Overland flow velocity may be estimated by combining a kinematic wave approximation with Manning's equation. The overland flow travel time, t_o (sec), for steady flow is given by kinematic wave equation (Chow et al., 1988):

$$t_0 = \frac{L^{0.6} n^{0.6}}{i_e^{0.4} S_0^{0.3}} \tag{11}$$

where i_e is the excess rainfall intensity (m/sec), L is the length of the overland flow (m), n is the Manning's roughness coefficient (Table 2 and Figure 6) and S_o is the slope (m/m). The rainfall intensity (i_e) in Equation 11 is determined from the sum of the cell excess rainfall determined by the

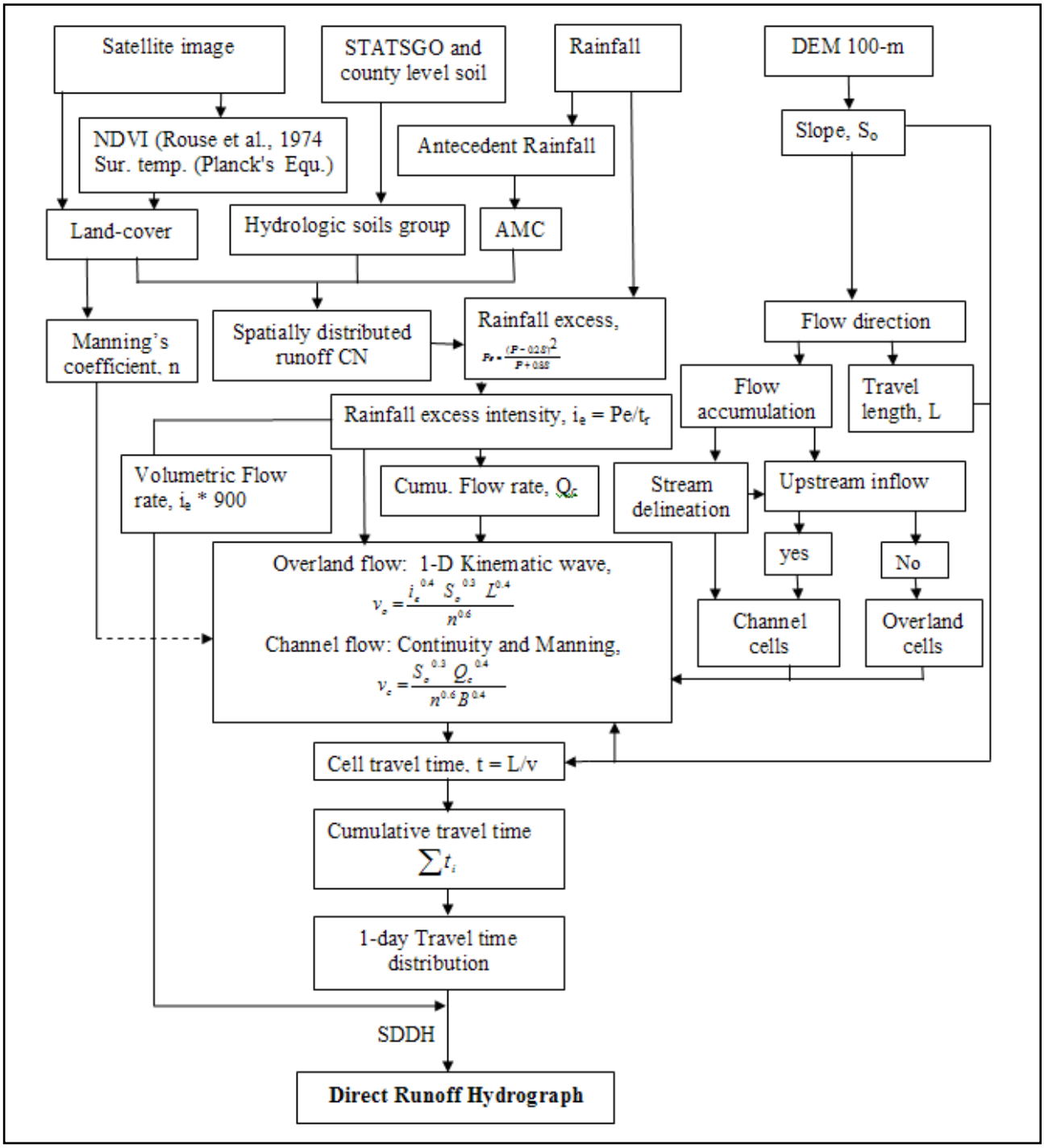

Figure 5. Runoff hydrograph computation flow chart.

CN method. For 100-m DEM grid size, the overland flow distance is 100 m for cells with horizontal or vertical flow directions and is 141 m for cells with diagonal flow directions. The derivation of the overland flow travel time using the kinematic wave approximation of the momentum equation and the continuity equation is shown in the Appendix.

Channel flow

The channel flow velocity, V_c (m/sec) (Equation 14) is computed using the continuity equation for a wide channel (Equation 13) and the Manning's equation (Equation 12). Open channel flow is assumed in the wide channel and the hydraulic radius is approximated by the depth of flow assuming

Table 2. Manning's Roughness Coefficients

Land-use	Manning's coefficient , n	Source
Developed	0.015	Montes, 1998
Cropland	0.040	Montes, 1998
Rangeland	0.07	Montes, 1998
Forest	0.200	Montes, 1998
Barrenland	0.055	Brater and King, 1976

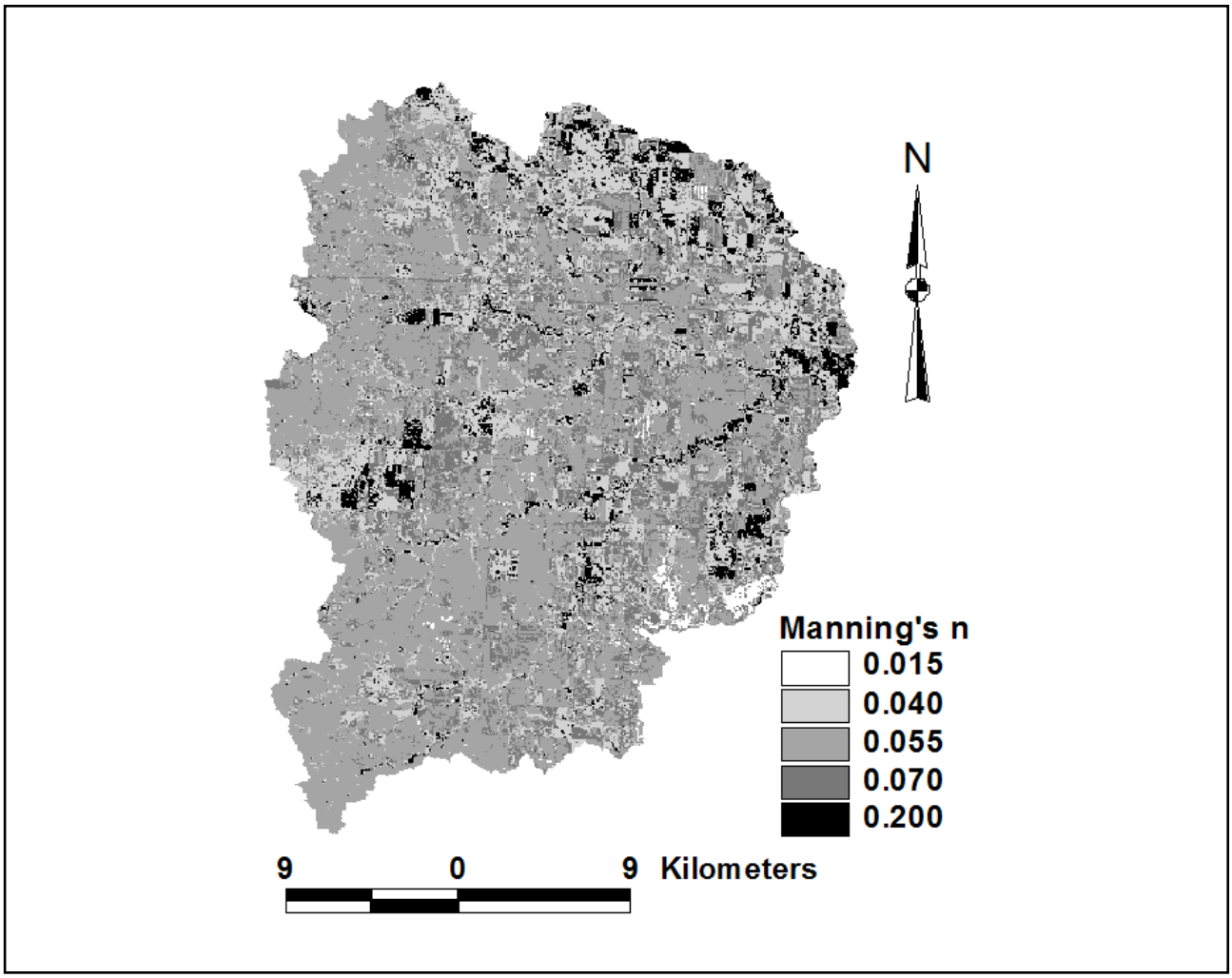

Figure 6. Manning's roughness coefficients.

the depth of flow is much smaller than the channel width.

$$V_c = \frac{S_0^{1/2}}{n} y^{2/3} \tag{12}$$

$$Q_c = V_c B y \tag{13}$$

$$V_c = \frac{S_0^{0.3}}{n^{0.6}} \left(\frac{Q_c}{B} \right)^{0.4} \tag{14}$$

where y is the depth of flow (m), Q_c is the cumulative discharge (m^3/s), B is the channel width (m), and n and S_o are defined as in Equation 11. Channels are assumed to have a rectangular cross-section with y depth of flow and an effective width of 1 m on average. This effective width was found through sensitivity analysis and gave the best predictions (Melesse, 2002). Discharge is determined from the total inflow into the cell, i.e., the rainfall excess intensity of a cell and inflows from upstream cells are summed and multiplied by the area of a cell (10,000 m^2). This is an approximation and the 1-D channel flow velocity derivation assumes no inflow. The flow accumulation request, an ArcView Avenue script to compute the upstream contributing areas, was modified to compute the cumulative discharge for each cell.

The travel time for each channel cell is computed from the cell velocity and the travel distance of the runoff water in the cell (Equation 15). Depending on the direction of flow for a 100-m cell size, the travel distance is 100 m for cells having horizontal or vertical flow directions and 141 m for cells having diagonal flow directions.

$$t_c = \frac{L}{v_c} \tag{15}$$

where t_c is the channel cell travel time (sec) and L is travel distance (m).

The cumulative travel time of the storm runoff to the watershed outlet was computed by summing the travel times along the unique flow-path from each cell following the flow directions. An ArcView Avenue script was developed to compute the overland and channel flow velocities, compute cumulative travel time, reclassify the cumulative travel time into 1-day intervals, and compute the corresponding watershed area drained for each travel time. From the travel time distribution and cell volumetric flow (i_e*A), direct runoff hydrographs were developed.

Direct Runoff Hydrograph

Spatially Distributed Direct Hydrographs (SDDHs) were developed directly based on the travel time distribution concept without using the unit hydrograph. The travel time of each cell to the outlet is computed and the volumetric flow is computed as the area of the cell multiplied by the respective excess rainfall. The direct runoff flow at the outlet is the sum of the volumetric flow from all cells arriving at the outlet at each respective travel time. This approach preserves the spatially distributed excess rainfall information, unlike the time-area method which ultimately requires a constant rainfall excess over the entire watershed. The predicted hydrograph was plotted together with the observed flow for comparison.

Model Comparison

The performance of the SDDH model was evaluated using the statistical comparisons of the predicted and observed hydrographs. Prediction of total runoff volumes, peak flow rates, time to peak, and model efficiency were used for comparison.

Most measures of goodness of fit used in hydrograph simulation have been based on the sum of squared errors, or error variance. Taking the squares of the residuals results in a positive contribution of both over-predictions and under-predictions. The error variance σ^2_ε, is defined as

$$\sigma_{\varepsilon}^2 = \frac{1}{n-1}\sum_{i=1}^{n}(Q_i(t) - Q_{si}(t))^2 \tag{16}$$

where $Q_{si}(t)$ is the simulated value of observed $Q_i(t)$ at time step i and n is the total number of time steps.

Another widely used goodness-of-fit measure based on the error variance is the model efficiency (E) (Nash and Sutcliffe, 1970), defined as

$$E = \left[1 - \frac{\sigma_{\varepsilon}^2}{\sigma_o^2}\right] \tag{17}$$

where $\sigma^2{}_o$ is the variance of the observed flow rate of each storm defined as

$$\sigma_o^2 = \frac{1}{n-1}\sum_{i=1}^{n}(Q_i(t) - \overline{Q_o})^2 \tag{18}$$

where $\overline{Q}_0$ is average observed flow rate for each storm.

RESULTS AND DISCUSSION

Land-cover mapping

From ISODATA unsupervised classification (Tou and Gonzales, 1974) 30 classes were generated. Recoding of the 30 classes to five land-cover classes was carried out with the scattergram of $NDVI_s$ and T_s (Figures 7 and 8).

The T_s- $NDVI_s$ slope is negative (Figure 7). The increase in green biomass is often associated with a reduction in surface resistance to evapotranspiration, greater transpiration, and a larger latent heat transfer resulting in lower surface temperature. The T_s-$NDVI_s$ scattergram shows a clear discrimination of land-cover classes and aggregation of classes with similar spectral signatures.

Surface temperature variation in vegetated surfaces (agriculture vs. range land) results from variations in the proportion of surrounding bare soil visible to the thermal sensor of Landsat and the thermal inertia of the surface (the measure of thermal response of surfaces to temperature changes). It is a function of thermal conductivity and heat capacity, and is affected by surface characteristics such as soil moisture and albedo. The thermal inertia of vegetation canopies is lower than that of soils.

Comparison of Observed and Predicted Runoff Volume

Runoff volume from the CN (Figure 9) computed using NRCS-CN method (infiltration excess) was estimated. From observed daily runoff hydrographs at the Heart River outlet, observed runoff depth was calculated as the area under the hydrograph curve divided by the watershed area. This was compared to the predicted total runoff volume estimated using the NRCS-CN technique. The residuals were computed as observed minus predicted. Comparison of these results (Figure 10) indicates that the NRCS-CN technique predicts the observed runoff volume with residual mean and standard deviation of -1.44 mm and 5 mm, respectively.

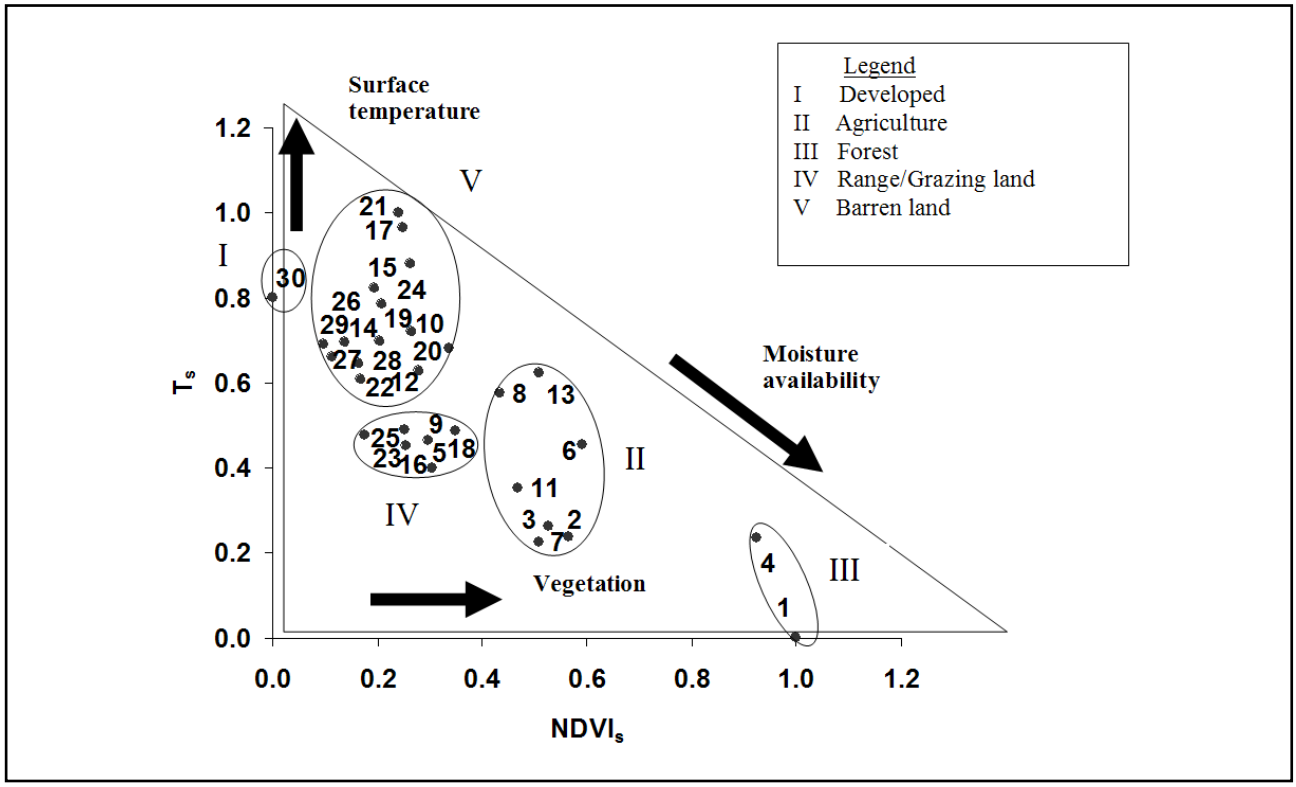

Figure 7. T_s vs. $NDVI_s$ scattergram.

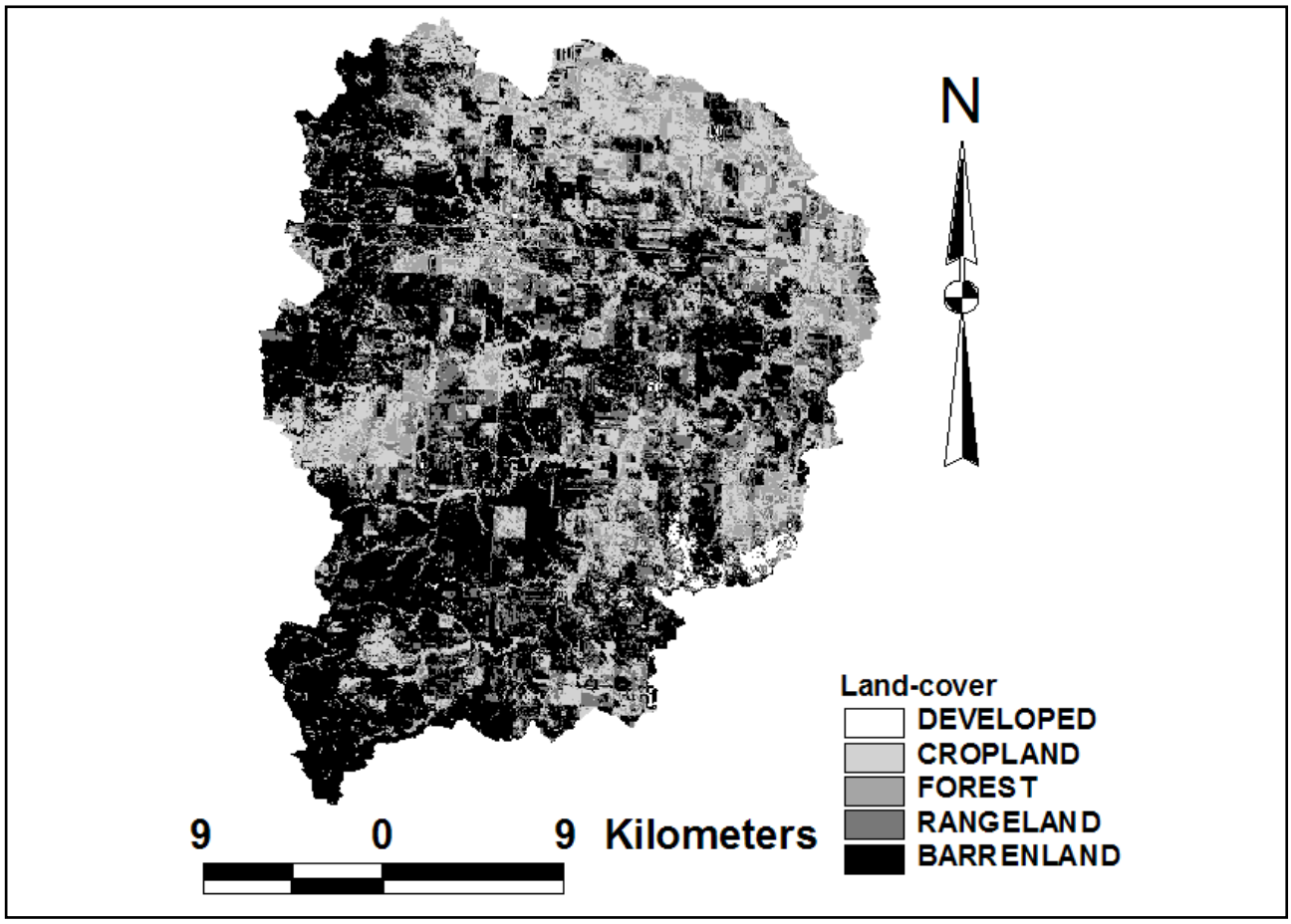

Figure 8. Land-cover from 2002 Landsat ETM+image.

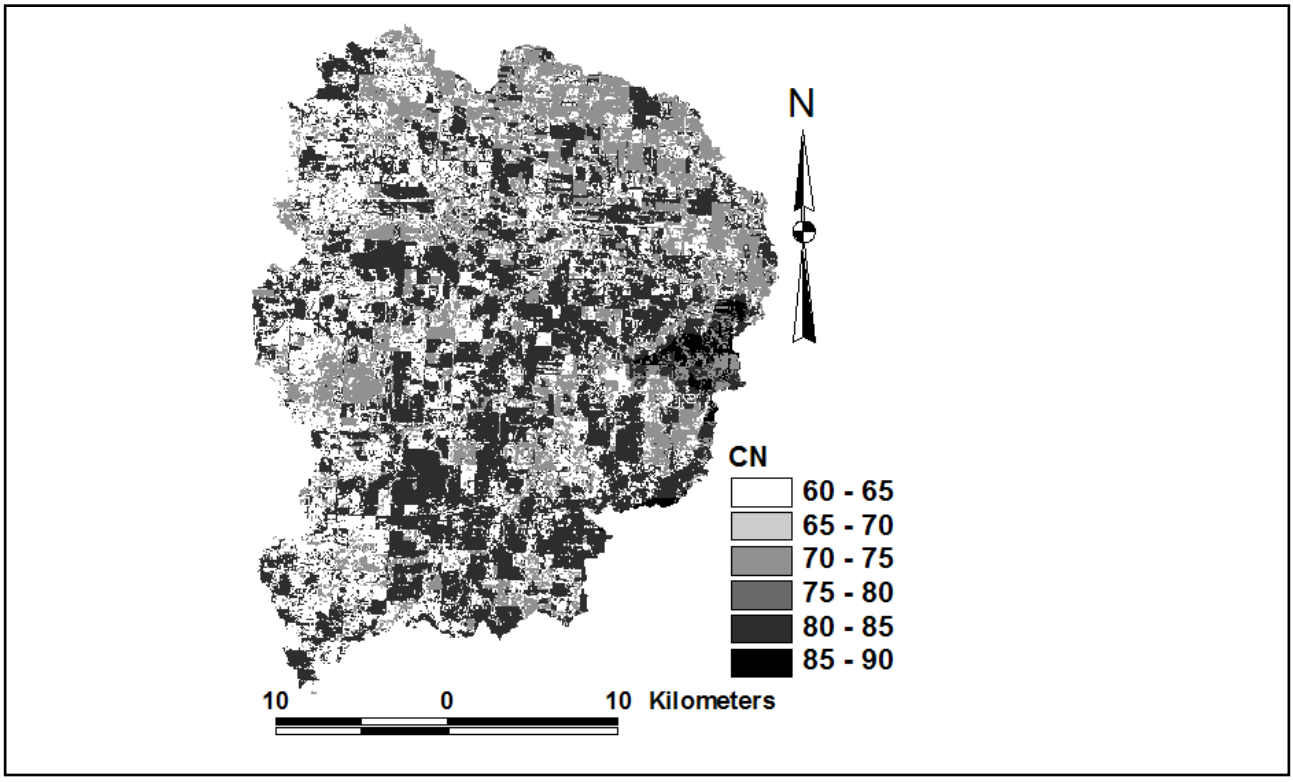

Figure 9. Curve Number from 2000 land-cover.

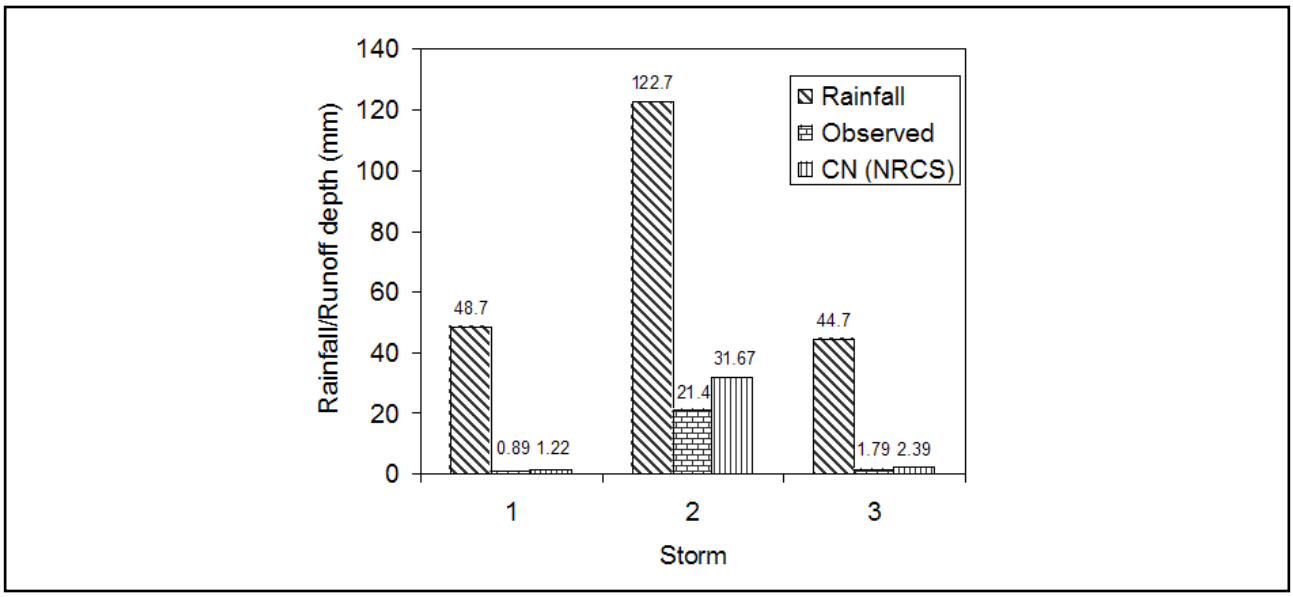

Figure 10. Comparison of runoff volumes.

Runoff Hydrographs

Runoff hydrograph prediction was done for 3 rainfall events. Table 3 summarizes the statistical analysis of the results of model prediction.

The storm on June 1, 2002 (Storm # 1) has a magnitude of 48.78 and intensity of 6.97 mm/day. Peak flow and time to peak prediction errors by SDDH were –14.75% and -10% (Table 3 and Figure 11a). The overall hydrograph efficiency was 0.68.

The July 19, 2002 storm (Storm # 2) had a total volume of 122.68 mm and an intensity of

approximately 11.15 mm/day. It represents a rainfall event with high volume and intensity, and runoffvolume. The SDDH method predicted the peak flow (1.22 m^3/s) and time to peak (10 days) (Table 3 and Figure 11b) with –10.16% and -7.69% errors (Table 3). The SDDH model efficiency was low with poor performance (0.04)

Table 3. Model Prediction and Performance Statistics

Storm number	Date	Observed			SDDH			
		Peak (m^3/s)	Time to peak (day)	Volume (mm)	Peak (m^3/s)	Time to peak (day)	Volume (mm)	Efficiency
1	01-Jun-02	1.22	10	0.92	1.4	11	1.22	0.68
2	19-Jul-02	49.13	13	21.38	54.12	14	31.67	0.04
3	18-Aug-02	2.72	9	1.79	3.3	12	2.39	-0.75
Average Error					-1.44	-1.25	-2.80	
Average Error Std Deviation					2.38	1.26	5.00	

The August 18, 2002 storm (Storm # 3) had a volume of 44.77 mm with 8 days of duration. Both the peak flow and time to peak was fairly predicted. The SDDH predicted peak flow with -21.32% errors (Table 3 and Figure 11c). Time to peak error was -33.33%.

In general, the SDDH method performed well with average peak and time to peak errors of -15% and 17%, respectively. The runoff volume predictions were not as good as the peak and time to peak with average errors of prediction of -38%.

CONCLUSION AND RECOMMENDATIONS

The use of land surface thermal map and NDVI from Landsat ETM+ sensor to enhance land-cover mapping was demonstrated. In general, the mid-morning surface temperature is inversely proportional to NDVI, a measure of plant biomass and condition. This study contributes a technique to enhance land-cover mapping by classifying using NDVI and thermal map in the absence of ground truth data. This technique can be extended to other studies aimed at discriminating land-cover types.

Hydrographs predicted by the SDDH travel time approach were comparable to the observed values. To maximize the utility of spatially integrated satellite information, distributed hydrologic models based on a grid GIS are necessary. Runoff estimation using remotely-sensed data and GIS will be advantageous if study areas are large, in-situ data are not available and alternative land-use scenarios must be explored.

This study contributes a technique to predict stream flow based on runoff travel time within the watershed using spatially distributed data (rainfall, Manning's roughness, and land-cover). The method developed requires as inputs only DEM, rainfall, and land-cover, and can be used in a GIS environment to predict stream flow in ungaged watersheds.

To better assess the performance of the runoff routing technique, it is recommended that the model be tested on different watersheds of varying topography and land-use. The routing technique

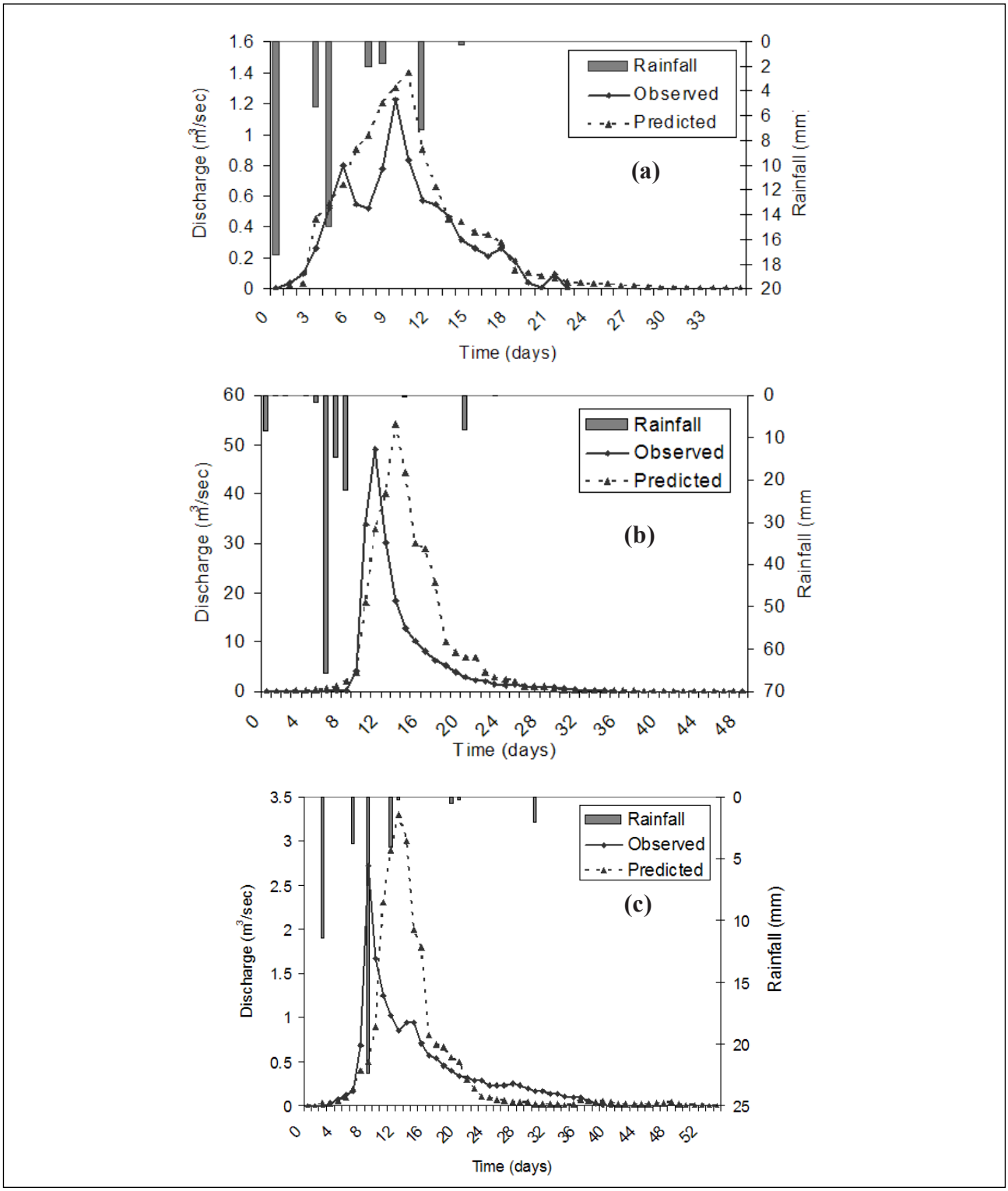

Figure 11. Predicted vs. observed runoff (a) Storm 1 (June 1, 2002), (b) Storm 2 (July 19, 2002), and (c) Storm 3 (August 18, 2002).

developed here does not consider storage effects of wetlands, lakes, and depressions. Including the effect of storage can significantly affect the time to peak and peak flow of predicted hydrographs, and this should be explored in future research. Since kinematic wave flow assumes friction and bed slope are identical, its applicability for flat topography is limited and using diffusive wave assumptions to estimate overland flow velocities should be explored.

ACKNOWLEDGMENTS

The author acknowledges George Seielstad for reviewing the paper and Vijay Nangia, Ofer Beeri, Grant Casady, David Baumgartner and other members of Upper Midwest Aerospace Consortium for their help. The author extends his appreciation to the USGS and North Dakota State Water Commission for providing elevation, rainfall and stream flow data.

REFERENCES

Ajward, M.H.; (1996). A Spatially Distributed Unit Hydrograph Model using a Geographical Information System. Ph.D. diss. Civil Engineering Dept., University of Calgary, Calgary, Alberta, Canada.

Anderson, J.R., E.E. Hardy, T.J. Roach, R.E. Witmer; (1976). A Land Use and Land Cover Classification System for use with Remote Sensor Data. U.S. Geological Survey Prof. Pap. 964, U.S. Gov. Printing Office, Washington. DC.

Arnold, J.G., R. Srinavasan, R.S. Muttiah, J.R. Williams; (1998). Large Area Hydrologic Modeling and Assessment. Part 1. Model Development. Journal of the American Water Resources Association. 34: 73-89.

Arnold, J.G., J.R. Williams; (1995). SWRRB-A Watershed Scale Model for Soil and Water Resources Management. Water Resource Publications, Highlands Ranch, CO, pp. 847-908.

Beasley, D.B., L.F. Huggins; (1981). ANSWERS Users Manual, EPA 905/9-82-001.U.S. Environmental Protection Agency, Chicago, IL.

Bedient, P.B., W.C. Huber; (1992). Hydrology and Floodplain Analysis, 2nd ed., Addison-Wesley, Reading.

Brater, E.F., H.W. King; (1976). Handbook of Hydraulics for the Solution of Hydraulic Engineering Problems. New York, McGraw-Hill Book Company.

Carlson, T.N., A.J. Ripley; (1997). On the Relationship between Fractional Vegetation Cover, Leaf Area Index and NDVI. Remote Sensing in Environment 62: 241-252.

Chow, V.T., D.R. Maidment, and L.W. Mays; (1988). Applied Hydrology, McGraw-Hill Inc., New York.

Djokic, D., D.R. Maidment; (1991). Terrain analysis for storm water modeling. Hydrologic Processes 5: 115-124.

Earth Resources Data Analysis System (ERDAS); (1999). ERDAS Field Guide, 5th ed., ERDAS Inc, Atlanta, GA, 671.

Flugel, W.A.; (1995). Delineating Hydrological Response Units (HRU's) by GIS Analysis for Regional Hydrological Modeling using PRMS/MMS in the Drainage Basin of the River Broel, Germany. Hydrological Processes 9: 423-436.

Gillies, R.R., T.N.Carson, W.P. Kustas, K.S. Humes; (1997). A verification of the 'triangle' method for obtaining surface soil water content and energy fluxes from remote measurements of the Normalized Difference Vegetation Index (NDVI) and surface radiant temperature, Int. J. Remote sensing 18: 3145-316.

Laflen, J.M., L.J. Lane, G.R. Foster; (1991). WEPP-A new Generation of Erosion Prediction Technology. Journal of Soil Water Conservation 46: 34-38.

Leonard, R.A., W.G. Knisel, D.A. Still; (1986). GLEAMS: Groundwater Loading Effects of Agricultural Management Systems. American Society of Agricultural Engineers. Paper No. 86-2511. Chicago, IL.

Maidment, D.R.; (1992a). Grid-based Computation of Runoff: A Preliminary Assessment, Hydrologic Engineering Center, US Army Corps of Engineers, Davis, California, Contract DACW05-92-P-1983.

Maidment, D.R.; (1992b). A Grid-Network Procedure for Hydrologic Modeling, Hydrologic Engineering Center, US Army Corps of Engineers, Davis, California, Contract DACW05-92-P-1983.

Maidment, D.R.; (1993a). Developing a Spatially Distributed Unit Hydrograph by Using GIS. *In*: Hydro GIS 93, Kovar, K., and Nachtnebel, H.P.,(editors), Int. Assn. Sci. Hydrol. Pub. No. 211, pp 181-192.

Maidment, D.R.; (1993b). GIS and Hydrologic Modeling. *In:* Environmental Modeling with GIS. Goodchild, M.F.,. Parks, B.O., Steyaert, L., (editors), New York:Oxford University Press

Maidment, D.R., F. Olivera, A. Calver, A. Eatherral, W. Fraczek; (1996). A Unit Hydrograph Derived From a Spatially Distributed Velocity Field. Hydrological Processes 10: 831-844.

Markham, B.L., J.L. Barker; (1986). Landsat MSS and TM post calibration dynamic ranges, exoatmospheric reflectance, and at-satellite temperatures, EOSAT Landsat Technical Notes, 1: 3-8.

Melesse, A.M.; (2002). Spatially Distributed Storm Runoff Modeling using Remote Sensing and Geographic Information Systems. Ph.D. diss. Agri. and Bio. Engineering Dept., University of Florida, Gainesville, Florida.

Melesse, A.M., J.D. Jordan, W.D. Graham; (2001). Enhancing Land Cover Mapping using Landsat derived Surface Temperature and NDVI. World Water and Environmental Resources Congress, American Society of Civil Engineers, May 20-24, 2001, Orlando, FL. (CD proceeding).

Moeller, R.A.; (1991). Application of geographic information system to hydrologic modeling using HEC-1. In: Stafford, D.B. (Ed.), Civil Engineering Applications of Remote Sensing and Geographic Information Systems. ASCE, New York, NY, pp. 269-277.

Montes, S.; (1998). Hydraulics of Open Channel Flows, ASCE Press, Reston, VA, pp. 697.

Moore, I.D., R.B. Grayson; (1991). Terrain-Based Catchment Partitioning and Runoff Prediction Using Vector Elevation Data. Water Resources Research, 27: 1177-1191.

Mueschen, B., K. Steinnocher; (2000). Integration of Spectral and Spatial Classification Methods for Model Parameterization in the ARSGISIP Project. Proc. of the 28th Int. Symp. on Remote Sensing of Environment, Capetown, 27-31, March, 4 pp.

Muzik I.; (1995). GIS derived Distributed Unit Hydrograph, a New Tool for Flood Modeling. In Developments in Computer Aided Design and Modeling for Civil Engineering, Topping, B.H.V., (eds). Edinburgh, UK: Civil-Comp Press; 243-247.

Muzik I., S.J. Pomeroy; (1990). A Geographic Information System for Prediction of Design Flood Hydrographs. Canadian Journal of Civil Engineering 17: 965-973.

Nash, J. E., J.V. Sutcliffe; (1970). River Flow Forecasting Through Conceptual Models 1. A Discussion of Principles. Journal of Hydrology 10: 282-290.

Ogden, F.L.; (1997). CASC2D Reference Manual, Dept. of Civil & Environmental Engineering, U-37, University of Connecticut, Storrs, CT 06269, 106 pp.

Olivera, F., D.R. Maidment; (1999). Geographic Information Systems (GIS)-based spatially distributed model for runoff routing. Water Resources Res. 35: 1155-1164.

Ott, M., Z. Su, A.H. Schumann, G.A. Schultz; (1991). Development of a Distributed Hydrological Model for Flood Forecasting and Impact Assessment of Land-use Change in the International Mosel River Basin. Hydrology for the Water Management of Large River Basins, Proc. of the Vienna Symposium. IAHS Pub. No. 201.

Owen, T.W., T.N. Carlson, R.R. Gillies; (1998). Remotely-sensed Surface Parameters Governing Urban Climate Change. Int. J. of Remote Sensing 19: 1663-1681.

Ragan, R.M., A.J. Kosicki; (1991). A geographic information system to support statewide hydrologic modeling with SCS-TR-20. In: Stafford, D.B. (Ed.), Civil Engineering Applications of Remote Sensing and Geographic Information Systems. ASCE, New York, NY, pp. 250-258.

Ridd, M.K.; (1995). Exploring a V-I-S (Vegetation-Impervious Surface-Soil) Model for Urban Ecosystem Analysis through Remote Sensing: Comparative Anatomy for Cities. Int. J. Remote Sensing 16: 2165-2185.

Rouse, J.W., R.H. Haas, J.A. Schell, D.W. Deering; (1974). Monitoring vegetation systems in the Great Plains with ERTS. Proc., Third Earth Resources Technology Satellite-1 Symposium, Greenbelt: NASA SP-351, 3010-3017.

Sasowsky, K.C., T.W. Gardner; (1991). Watershed configuration and geographic information system parameterization for SPUR model Hydrologic Simulations. Water Resources Res. 27: 7-18.

See, R.B., D.L. Naftz, C.L. Qualls; (1992). GIS Assisted Regression Analysis to Identify Sources of Selenium in Streams. Water Resources Bulletin 28: 315-330

Smith, M.B., M. Brilly; (1992). Automated grid element ordering for GIS-based overland flow modeling. Photogrammetric Engineering and Remote Sensing 58: 579-585.

Stuebe, M.M., D.M. Johnson; (1990). Runoff volume estimation using GIS techniques. Water Resources Bulletin 26: 611-620.

Tou, J.T., R.C. Gonzales; (1974). Pattern Recognition Principles. ISODATA Algorithm in Chapter 3, Pattern Classification By Distance Functions. Reading, MA: Addison-Wesley. pp. 97-104.

U.S. Army Corps of Engineers; (1985). HEC– Flood Hydrograph Package. Davis, CA.

USDA; (1980). CREAMS: A Field Scale Model for Chemicals, Runoff and Erosion from Agricultural Management Systems. Conservation Research Report No. 26, Southeast Area. Washington, D.C.

USDA, Soil Conservation Service;(1985). National Engineering Handbook, Section 4: Hydrology. U.S. Government Printing Office, Washington, DC.

USDA, Soil Conservation Service; (1986). Urban Hydrology for Small Watersheds. SCS Technical Release 55, U.S. Government Printing Office, Washington, DC.

USGS; (2003). http://nd.water.usgs.gov/pubs/key/r7.html (accessed June 20, 2003).

Vieux, B.E.; (2001). Distributed Hydrological Modeling Using GIS, Kluwer Academic Publishers.

Young, R.A., C.A. Onstad, D.D. Bosch, W.P. Anderson; (1985). Agricultural Non-point Surface Pollution Models (AGNPS) I and II Model Documentation. Pollution Control Agency, St. Paul, and U.S Department of Agriculture. Agricultural Research Service Washington, D.C.

ADDRESS FOR CORRESPONDENCE
Assefa M. Melesse
Assistant Professor
Earth Systems Science Institute
University of North Dakota
Grand Forks, ND 58202
USA

Email:assefa@aero.und.edu

NOTATION

B	channel width (m)
CN	curve number
DN	digital number
F	actual retention after runoff begins (mm)
I	initial abstraction (mm)
i_e	excess rainfall intensity (m/sec)
K_1	calibration constant 1 ($Wm^{-2}sr^{-1}mm^{-1}$)
K_2	calibration constant 2 ($Wm^{-2}sr^{-1}mm^{-1}$)
L	flow length (m)
L_{max} and L_{min}	maximum and minimum spectral radiance, ($Wm^{-2}ster^{-1}mm^{-1}$)
$NDVI$	normalized difference vegetation difference
n	Manning's roughness coefficient
$NDVI_{low}$ and $NDVI_{high}$	lowest and highest normalized difference vegetation difference
$NDVI_s$	scaled Normalized Difference vegetation difference
NIR	near infrared band
P	total rainfall (mm)
Q	actual direct runoff (mm)
Q_c	cumulative discharge (m^3/s)
$Q_i(t)$	observed flow at time step i (m^3/s)
$Q_{si}(t)$	simulated flow at time step i (m^3/s)
$\overline{Q}_0$	average observed flow rate (m^3/s)
R	spectral radiance ($Wm^{-2}sr^{-1}mm^{-1}$)
RED	red band
S	watershed storage (mm)
S_o	slope (m/m).
T	surface temperature (^oK)
t_c	channel flow travel time (sec)
T_{high} and T_{low}	highest and lowest surface temperature (^oK)
t_o	overland flow travel time (sec)
T_s	scaled surface temperature
V_c	channel velocity (m/sec)
y	depth of flow (m)
σ^2_o	variance of the observed flow rate
$\sigma^2\varepsilon$	error variance

APPENDIX

Derivation of Kinematic Wave Overland and Channel Flow Velocities

The 1-D continuity equation for overland or channel flow is

$$\frac{\partial Q}{\partial x}+\frac{\partial A}{\partial t}=i_e \tag{A.1}$$

where Q = volumetric discharge (L^3/T), A = cross-sectional flow area (L^2), i_e = inflow (lateral or rainfall) (L/T)

For the kinematic wave assumption, the momentum equation reduces to

$$S_f = S_o \tag{A.2}$$

where S_f = friction slope, S_o = bed slope

Manning's equation can be used to describe friction loss, S_f (Chow et al., 1988),

$$v=\frac{1}{n}R^{2/3}S_f{}^{1/2} \qquad \text{(SI units)} \tag{A.3}$$

where v = velocity (L/T), R = hydraulic radius (L), and n is the manning's coefficient.

1-D overland Flow

For 1-D overland flow, the continuity equation is obtained by rewriting Equation A.1 in terms of flow per unit width for overland flow,

$$\frac{\partial q}{\partial x}+\frac{\partial y}{\partial t}=i_e \tag{A.4}$$

where i_e = rate of excess rainfall (L/T), $q_o = vy_o = Q/B$ = flow per unit width (L^2/T)

For overland flow, $R = y$, thus Manning's equation, Equation A.3 reduces to

$$v=\frac{1}{n}y^{2/3}S_f{}^{1/2} \tag{A.5}$$

In general equation A.5 can be rewritten in the form,

$$v=\alpha_o y_o{}^{m_o} \tag{A.6}$$

thus

$$q_o = vy_o = \alpha_o y_o{}^{m_o+1} \tag{A.7}$$

Substituting Equation A.7 in to Equation A.4

$$\frac{\partial(\alpha_o y_o{}^{m})}{\partial x}+\frac{\partial y_o}{\partial t}=i_e \tag{A.8}$$

where $m = m_o + 1$

Simplifying this equation gives,

$$\alpha_o m\, y_o^{m-1} \frac{\partial y_o}{dx} + \frac{\partial y_o}{\partial t} = i_e \tag{A.9}$$

where $\alpha_o y_o^{m-1}$ can be interpreted as the celerity, c, of the kinematic wave (Bedient and Huber, 1992).

When moving with the wave speed, c (Bedient and Huber, 1992),

$$c = \frac{dy_o}{dt} = \frac{dx}{dt}\frac{\partial y_o}{\partial x} + \frac{\partial y_o}{\partial t} = i_e \tag{A.10}$$

Since

$$\frac{dx}{dt} = \alpha_o y_o^{m-1} \tag{A.12}$$

$$\frac{dy_o}{dt} = \alpha_o y_o^{m-1} \frac{\partial y_o}{\partial x} + \frac{\partial y_o}{\partial t} = i_e \tag{A.13}$$

Therefore the relation between depth of flow and rainfall excess is given by,

$$\frac{dy_o}{dt} = i_e \tag{A.14}$$

Integrating Equation. A.14 for an initially dry surface ($y_o(t=0)=0$),

$$y = i_e t \tag{A.15}$$

Substituting equation E.15 into equation E.12 and integrating yields,

$$x = x_o + \alpha_o i_e^{m-1} t_o^{m} \tag{A.16}$$

Solving for t_o,

$$t_o = \left[\frac{L_o}{\alpha_o i_e^{m-1}}\right]^{1/m} \tag{A.17}$$

where $x - x_0 = L_o$ = overland flow length (L), t_o = overland flow time (T)

For Manning's equation the parameters m and a_o are given by (Bedient and Huber, 1992),

$$m = \frac{5}{3} \tag{A.18}$$

$$\alpha_o = \frac{1}{n}\sqrt{S_o} \qquad \text{(SI units)} \tag{A.19}$$

Substituting Equation. A.18 and A.19 to Equation A.17 yields,

$$t_0 = \frac{L^{0.6} n^{0.6}}{i_e^{0.4} S_o^{0.3}} \tag{A.20}$$

where t_o is overland flow time (sec), L is overland flow length (m), n is manning's roughness coefficient , i_e is rainfall intensity excess (m/sec) and S is slope (m/m).

The overland flow velocity can be approximated as

$$V_o = \frac{L}{t_o} \tag{A.21}$$

$$V_o = \frac{S_o^{0.3} (i_e L)^{0.4}}{n^{0.6}} \tag{A.22}$$

1-D Channel Flow

For 1-D channel flow with no inflows, the continuity equation is given by,

$$\frac{\partial Q}{\partial x} + \frac{\partial A}{\partial t} = 0 \tag{A.23}$$

If the flow is steady, $\frac{\partial A}{\partial t} = 0$. Thus $\frac{\partial Q}{\partial x} = 0$, indicating Q is constant.

In this case the continuity equation reduces to,

$$Q = vA = vBy \tag{A.24}$$

$$y = \frac{Q}{vB} \tag{A.25}$$

Where B is channel flow width (L) and Q is a cumulative discharge (L^3/T), computed as the sum of volumetric inflow from upstream cells.

For a wide channel ($R = y$) and substituting Equation A.25 in Equation A.5 yields,

$$v = \frac{1}{n}\left(\frac{Q}{vB}\right)^{2/3} S_o^{1/2} \tag{A.26}$$

Solving for v yields

$$v = \frac{S_o^{0.3}}{n^{0.6}}\left(\frac{Q}{B}\right)^{0.4} \tag{A.27}$$

Equation A.22 and A.27 are the overland and channel flow velocities, respectively. Both equations are dependent on the slope, $S_o^{0.3}$ and manning coefficient, $n^{-0.6}$. The overland velocity is also dependent on the excess rainfall intensity, i_e, and flow distance L, whereas the channel velocity is a function of channel width, B and cumulative discharge, Q.